Study of low-P_T spectra, sea and valence quark distributions, and correlations in 50-GeV/c π^-—emulsion-nuclei interactions

Chandra Gupt and R. K. Shivpuri
Department of Physics and Astrophysics, University of Delhi, Delhi 110007, India

N. S. Verma and A. P. Sharma
Department of Physics, Kurukshetra University, Kurukshetra 132119, India
(Received 13 June 1980; revised manuscript received 20 October 1981)

The low-P_T region of secondary pions, the sea and valence quark distributions in the projectile and the target, and rapidity correlations among secondary pions are investigated in interactions of 50-GeV/c π^- with nuclear emulsion placed in a strong magnetic field. The existence of a sharp peak in the region of $P_T^2 \leq 0.12$ (GeV/c)^2 for positive and negative pions in the forward and backward hemispheres in the center-of-mass system is explained on the basis of resonance formation. The production of secondary pions is explained on the basis of the quark-antiquark-recombination model. We have used the valence and sea quark distributions in the pion for explaining the π^+/π^- ratio. We find an enhancement in the number of sea quarks with an increase in nuclear-target size. Single-particle and two-particle inclusive rapidity distributions have been studied. The rapidity-difference distributions and the normalized correlation function R have also been investigated. It is found that no positive correlations among secondary pions are evident at this primary energy.

I. INTRODUCTION

Interactions with nuclear targets at high energies has become a topic of considerable interest in recent years. The reason for this interest is manifold. Such a study will provide information about the space-time evolution of hadronic final states. We can understand how the h-h interaction is modified by the presence of other nucleons in the target. The role of the nucleons in multiparticle production processes can also be gauged in these interactions. The quark structure functions of the projectile and the target can also be determined. In this paper, we study the low-P_T spectra of the secondary particles, the sea and valence quark distributions in the projectile and the target, and finally the correlations among the secondary particles at 50 GeV/c π^- interactions with emulsion nuclei. The justification for this kind of study is given in the following paragraphs.

The production of resonances has played a dominant role in high-energy interactions. It is, therefore, natural to explain all the interaction characteristics in terms of the resonant states. A parameter of singular importance in high-energy interactions is the low transverse momentum (P_T) of the secondary particles. Its uniqueness lies in its strong damping and invariant distribution with respect to the primary energy and kind of primary particle. Due to its invariant characteristics, it was considered to be an uninteresting parameter. However, in the last few years, attempts have been made to relate the low-P_T behavior to the mechanism of particle production. An interesting work on this aspect is that of Yen and Berger[1] who have shown that the steep forward peak in P_T can be attributed to the decay of nucleon resonances produced peripherally. It would be quite interesting to explain the low-P_T behavior at different primary energies following this prescription. This approach is all the more attractive since even the large-P_T behavior has been accounted for on the basis of the formation of clusters[2] (generalized resonances). Hence, there exists a possibility of developing a unified approach to the low- and high-P_T phenomena.

Recently the quark-antiquark-recombination model of Das and Hwa[3] has been applied successfully to single-particle inclusive hadron production in the low-P_T region. According to this model[3–7] a valence quark (antiquark) picks up an antiquark (quark) from the sea to form a meson at low P_T.

The recombination of quarks and antiquarks from the sea accounts predominantly for the production of mesons in the nondiffractive low-P_T region. Duke and Taylor[4] have used this recombination process to explain the production of various hadrons in p-p collisions. The model has been extensively applied by Biswas *et al.*[5] for determining valence and sea quark distribution functions of the pion in $\pi^- p$ interactions at 200 GeV/c. DeGrand and Miettinen[6] have predicted the cross section of secondary pions produced in association with a massive dilepton pair on the basis of this model. Until now low-P_T meson production in hadron-nucleon interactions alone has been studied on the basis of the recombination model. It would be interesting to apply this model to hadron-nucleus interactions also.

The existence of correlations among the secondary particles produced in nucleon-nucleon or nucleon-nucleus interactions at high energies has been clearly established in the last few years by a number of investigators.[8] Correlations and cluster production has played a dominant role in understanding the basic features of multiparticle production in high-energy interactions. Experiments at Fermilab and CERN ISR have found correlations to be nonzero and positive over some regions of the phase space. Correlations are present because the secondary particles are the decay products of a mass of nuclear matter called a cluster, produced at the point of interaction. The idea of the independent emission of clusters is applied in understanding the observed positive short-range two-particle rapidity correlations in the central region.

Most of the investigations[8] on correlations have been carried out at very high energies (>100 GeV/c). In an earlier work[9] at cosmic-ray energies (0.1—2600 TeV), some of us have shown the dependence of cluster size and strength of correlation on primary energy. It was found that with in-

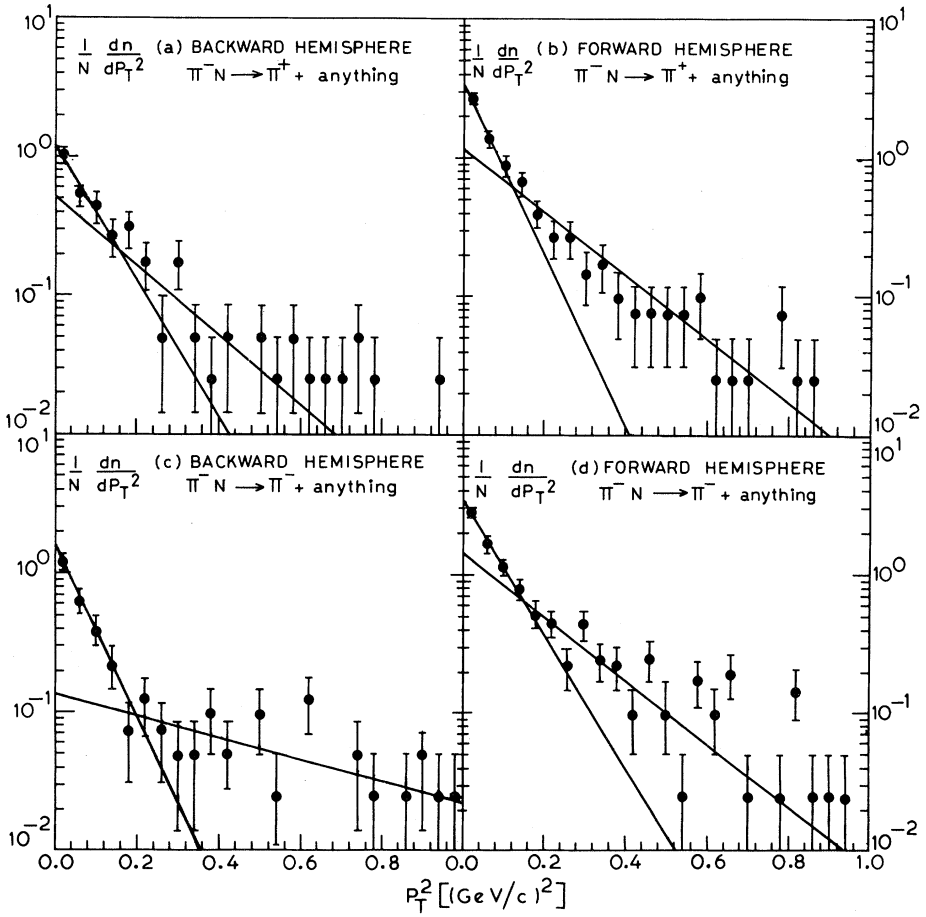

FIG. 1. P_T^2 distributions of positive secondary pions in (a) backward and (b) forward hemispheres and of negative secondary pions in (c) backward and (d) forward hemispheres in $\pi^- N$ interactions. The forms of the solid lines which represent best fits to the data are described in the text and their values are given in Table I.

creasing primary energy the correlations among the secondary particles become stronger and the size of the cluster also becomes larger. It would be interesting to investigate whether positive correlations are present in interactions at lower energies.

The experimental details of the present work are given in Sec. II. In Sec. III A, the low-transverse-momentum distributions are studied for three classes of events, namely, (i) $n_h=0,1$, (ii) $n_h=2,3,4$, and (iii) $n_h\geq 8$, where n_h is the heavy-prong multiplicity. The P_T distributions of positive and negative pions have been studied separately. The distributions have been further studied for forward and backward hemispheres in the center-of-mass system which is essentially the projectile fragmentation region and the target fragmentation region, respectively. We find an existence of a sharp peak for $P_T{}^2\leq 0.12$ (GeV/c)^2 for all the three classes of interaction. This characteristic is explained on the basis of decay of nucleon resonances produced peripherally. We have also obtained information about sea and valence quark distributions in the pion and in the emulsion nuclei. Our sea and valence quark distributions in the pion compare well with those obtained by Biswas *et al.*[5] and our sea and valence quark distributions in the emulsion follow the same form as those of Duke and Taylor.[4] In Sec. III B, the details of the recombination model at small x ($x\leq 0.5$) are given. We also discuss the various π^+/π^- ratios as functions of x in Sec. III B. These π^+/π^- ratios are well explained on the basis of the recombination model. In Sec. III C, we investigate the existence of correlations in these interactions. We find that no positive correlations are evident among the secondary particles at the level of statistics of the present experiment. This result is consistent with an earlier paper[9] where the

TABLE I. The values of the slopes which are the best fits to the data are given for positive and negative secondary pions produced in forward and backward hemispheres for the three classes of interactions. A is the value of the sharp slope, whereas B is the value of shallow one. The values of χ^2 per degree of freedom (DOF) for A and B are also given.

Reaction	Backward hemisphere A	χ^2/DOF	B	χ^2/DOF	Forward hemisphere A	χ^2/DOF	B	χ^2/DOF
Figs. 1(a), 1(b) $\pi^-N\to\pi^+ +$ anything	-11.5 ± 0.6	0.81/3	-5.8 ± 0.6	15.04/17	-14.4 ± 1.6	0.47/3	-5.8 ± 0.7	8.27/18
Figs. 1(c), 1(d) $\pi^-N\to\pi^- +$ anything	-14.7 ± 0.2	0.12/3	-1.8 ± 0.2	9.59/17	-11.2 ± 0.1	0.11/3	-5.3 ± 0.6	29.31/20
Figs. 2(a), 2(b) π^-CNO$\to\pi^+ +$ anything Target mass=CNO mass	-41.8 ± 0.1	0.000 01/2	-0.4 ± 0.8	0.38/5	-18.4 ± 1.7	0.51/3	-4.1 ± 0.6	16.45/21
Figs. 2(c), 2(d) π^-CNO$\to\pi^+ +$ anything Target mass=proton mass	-25.0 ± 3.2	0.66/3	-1.8 ± 0.5	13.29/15	-17.6 ± 4.0	1.86/3	-3.9 ± 0.4	13.34/21
Figs. 3(a), 3(b) π^-CNO$\to\pi^- +$ anything Target mass=CNO mass	-46.8 ± 0.1	0.000 002/2			-19.5 ± 2.9	1.91/3	-4.6 ± 0.6	20.25/21
Figs. 3(c), 3(d) π^-CNO$\to\pi^- +$ anything Target mass=proton mass	-31.2 ± 1.0	0.04/3	-0.9 ± 1.2	16.10/13	-16.3 ± 3.0	1.63/3	-4.5 ± 0.6	15.03/21
Figs. 4(a), 4(b) π^-AgBr$\to\pi^+ +$ anything Target mass=AgBr mass	-36.8 ± 10.0	1.19/3	-0.1 ± 1.2	1.93/9	-17.3 ± 2.7	3.74/3	-4.4 ± 0.5	24.95/21
Figs. 4(c), 4(d) π^-AgBr$\to\pi^+ +$ anything Target mass=proton mass	-23.8 ± 4.4	4.54/3	-4.5 ± 0.7	19.94/21	-11.0 ± 1.0	0.21/3	-5.0 ± 0.7	19.71/21
Figs. 5(a), 5(b) π^-AgBr$\to\pi^- +$ anything Target mass=AgBr mass	-44.8 ± 0.1	0.000 01/2			-15.5 ± 2.0	1.92/3	-3.7 ± 0.3	23.53/22
Figs. 5(c), 5(d) π^-AgBr$\to\pi^- +$ anything Target mass=proton mass	-23.6 ± 5.8	4.98/3	-4.1 ± 0.8	19.27/20	-11.1 ± 0.4	0.04/3	-3.6 ± 0.4	21.86/21

dependence of correlations on primary energy had been shown. It seems that the primary energy in the work reported here is low, so that the correlations are not seen. We discuss below the various single-particle and two-particle inclusive distributions. The rapidity-difference distributions and the normalized correlation function R are also discussed.

II. EXPERIMENTAL DETAILS

Four NIKFI-R emulsion stacks were exposed to a 50-GeV/c π^- meson beam under a pulsed magnetic field having a strength of about 170 kG at the Serpukhov accelerator. The pulsed magnetic field was produced with the Mamont set-up[10] constructed at CERN. The direction of the magnetic field was kept perpendicular to the beam direction which had a momentum spread of 1%. After a careful selection of the primary interactions the momentum of the secondary shower particles ($\beta \geq 0.7$) produced have been measured using the magnetic curvature technique described by Tolstov and Shabratova.[11] In this technique the three-point deflection method as described by Danysz[12] *et al.* has been used. On each track the Y coordinates of three equally spaced points were noted. The deflection (D) of the track is related to the strength of the magnetic field (H) and the particle momentum (P) by the relation

$$P = \frac{3\times 10^{-4} H t^2}{D \cos\alpha} ,$$

where $D = Y_3 - 2Y_2 + Y_1$, i.e., second difference of the Y coordinates of the track, t = spacings be-

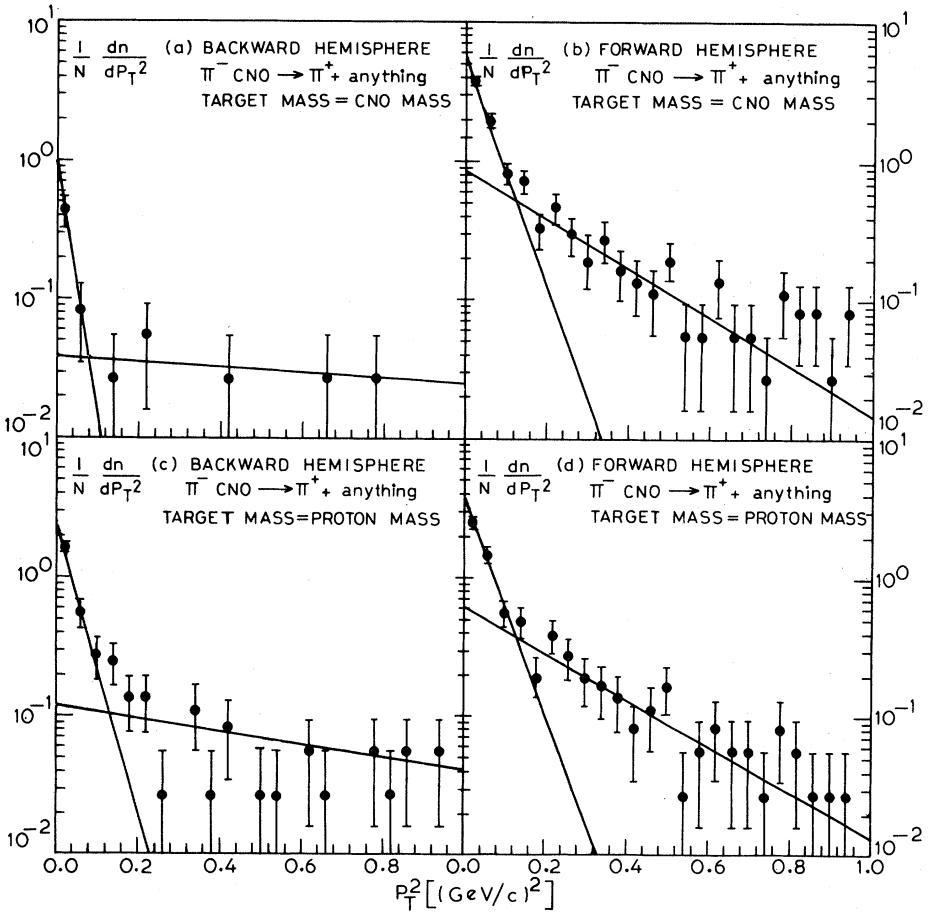

FIG. 2. P_T^2 distributions of positive secondary pions in (a) and (c) backward and (b) and (d) forward hemispheres in π^-CNO interactions. In (a) and (b) the target mass is equal to CNO mass, whereas in (c) and (d) the target mass has been taken equal to proton mass. The forms of the solid lines which represent best fits to the data are described in the text and their values are given in Table I.

tween the Y coordinates, and α = dip angle of the track.

Using the above relations, the effective value of the magnetic field $\langle H_{\text{eff}} \rangle$ has been calculated. The curvature of the primaries has been measured. The value of $\langle H_{\text{eff}} \rangle$ comes out to be $=167.5 \pm 3.54$ kG. The relative error on the momenta measurements is comprised of the errors due to magnetic-field intensity and distortions in the emulsion. Again, the error in D is due to the Coulomb scattering and the emulsion distortion. The Coulomb scattering is quite small compared to the scattering due to the strong magnetic field and hence its contribution can be neglected. It has been shown by Tolstov and Shabratova[11] that as a first-order approximation the distortion correction may not be taken into account in the case of strong magnetic fields ~ 100 kG for the particles of momenta ≤ 50 GeV/c in BR-2 emulsion (present stack). However in order to minimize the distortion effects we have adopted the following criteria in the selection of interactions. (i) The interactions lying in the middle pellicles of the emulsion have been chosen and hence the interactions lying within the 50 μm from the emulsion surface or 50 μm from glass side have been discarded. (ii) The cutoff limit on the edges is taken to be 5 grids all around.

The criteria for selection of tracks for measurements are as follows. (a) The available projected length should be greater than 500 μm. (b) Tracks which suffer more than one nuclear scattering at consecutive points less than 400 μm apart have not been considered. (c) Maximum possible track length is followed up. (d) The track segments lying within the 50-μm region either from emulsion surface or from glass surface have been discarded.

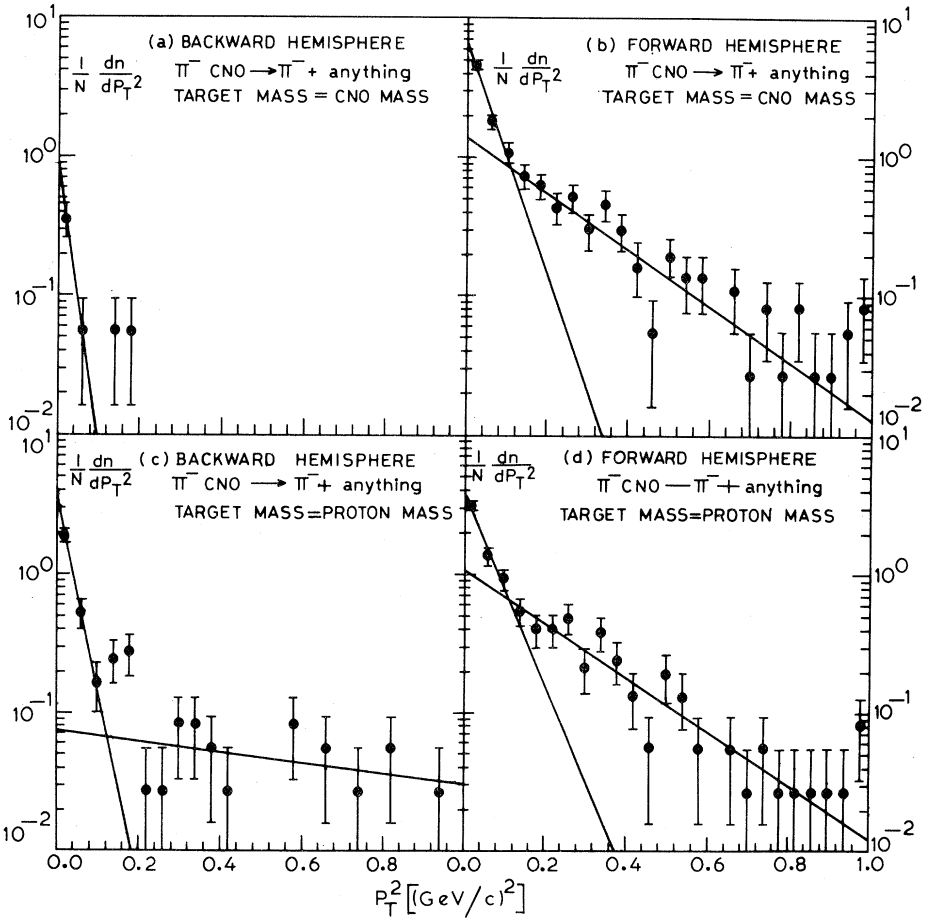

FIG. 3. P_T^2 distributions of negative secondary pions in (a) and (c) backward and (b) and (d) forward hemispheres in π^-CNO interactions. In (a) and (b) the target mass is equal to CNO mass whereas in (c) and (d) the target mass has been taken equal to proton mass. The forms of the solid lines which represent best fits to the data are described in the text and their values are given in Table I.

The charges of the shower particles were determined with the following criteria in mind. (1) All the produced secondary particles are singly charged. (2) The primary particles have negative unit charge.

Following the aforementioned criteria, the total number of events selected for measurement were found to be 846. The number of events having $n_h=0,1$, $n_h=2,3,4$, and $n_h\geq 8$ are found to be 233, 171, and 302, respectively. The average multiplicity of the events in the above three cases is 5.6, 7.1, and 10.7, respectively. These three type of interactions can be assumed to belong to nucleon, CNO, and AgBr targets, respectively. As is usual in emulsion experiments, events with $n_h=0,1$ have been assumed to be interactions with single nucleons of the target. This classification has been followed in an earlier work.[13] The $n_h=0,1$ events are either due to collisions with pure H nuclei or due to collisions with the heavy emulsion nuclei. In the latter type of collisions, since the events have zero or a very small momentum transfer to the nucleus, the interactions are effectively with a single nucleon and the rest of the nucleus remains a spectator during the collision. The production of fast secondary particles takes place only in the initial hadron-hadron collision. The larger the value of n_h, the larger is the contribution of nucleons to the collision process. The value of n_h reflects the number of nucleons that have participated in the interaction. Again, it has been shown earlier[14] that events with $n_h\leq 4$ have been considered to be hadron—light-nuclei (CNO) interactions. In order to ensure a high percentage of light-nucleus interactions in the sample, events with $n_h=5$, 6, and 7 have not been taken into account, since such

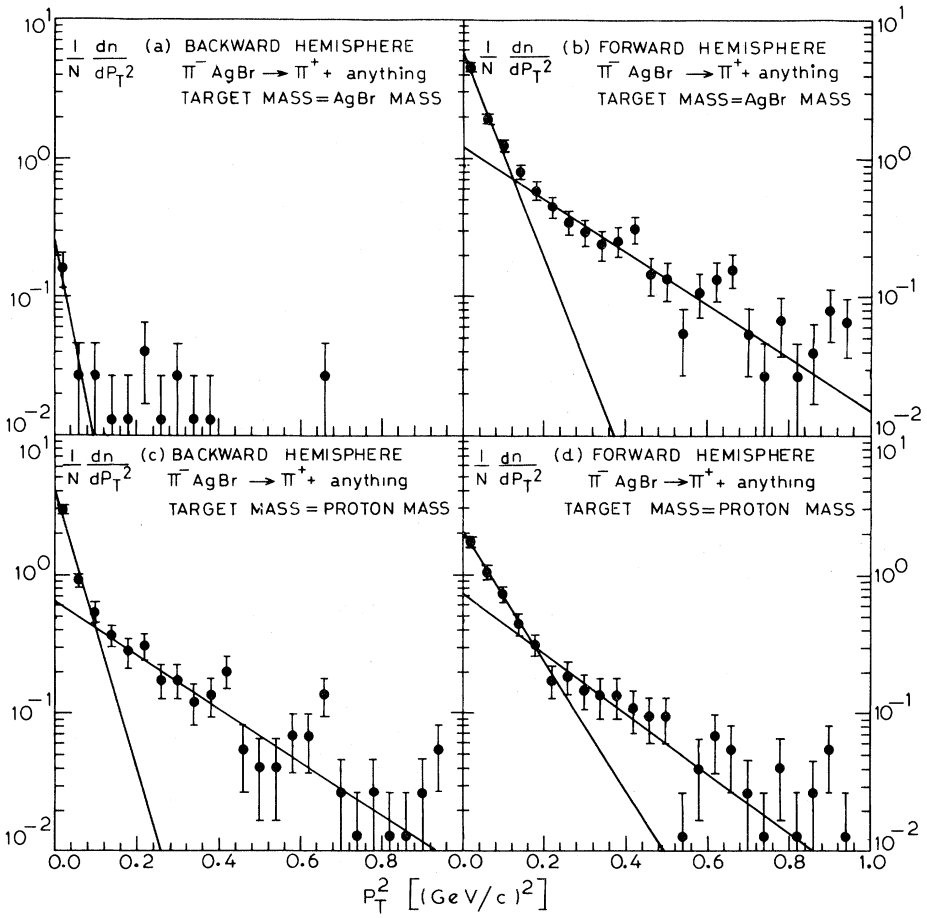

FIG. 4. $P_T{}^2$ distribution of positive secondary pions in (a) and (c) backward and (b) and (d) forward hemispheres in π^-AgBr interactions. In (a) and (b) the target mass is equal to the AgBr mass whereas in (c) and (d) the target mass has been taken equal to proton mass. The forms of the solid lines which represent best fits to the data are described in the text and their values are given in Table I.

events could also come from collisions with heavy nuclei. Events with $n_h \geq 8$ are clearly interactions with AgBr nuclei.[14] This paper is based on the largest statistics of the data at 50 GeV/c in nuclear emulsions reported so far.

III. RESULTS AND DISCUSSION

A. Low-transverse-momentum distributions

In Fig. 1 the transverse-momentum distributions of secondary positive and negative pions are plotted, for backward and forward hemispheres in the center of mass of pion-nucleon systems, respectively. In each of the four cases, a sharp peak $[\exp(AP_T^2)]$ is clearly indicated for $P_T^2 \leq 0.12$ $(\text{GeV}/c)^2$ and a shallow peak $[\exp(BP_T^2)]$ is observed for $P_T^2 > 0.12$ $(\text{GeV}/c)^2$. The values of A and B which yielded the lowest χ^2 are given in Table I for each case. The solid lines in the distributions are the best fits to the data. The values of χ^2 and χ^2/DOF for the exponential curves for different distributions are also given in Table I. The method adopted for calculating χ^2 values is the same as followed in an earlier paper.[15] It is evident from Table I that the values obtained have a fairly good confidence level.

In earlier work,[16] we observed a similar sharp peak $[\exp(-24P_T^2)]$ for $P_T^2 \leq 0.12$ $(\text{GeV}/c)^2$ and a shallow peak $[\exp(-3.1P_T^2)]$ for $P_T^2 > 0.12$ $(\text{GeV}/c)^2$ for charged pions in 22.8 GeV/c proton-nucleon interactions. Akerlof *et al.*[17] and Ratner *et al.*[18] have also observed similar sharp peaks. Akerlof *et al.*[17] have observed a sharp forward peak $[\exp(-15P_T^2)]$ for $P_T^2 \leq 0.12$ $(\text{GeV}/c)^2$ and a shallow peak $[\exp(-2.8P_T^2)]$ for $P_T^2 > 0.12$ $(\text{GeV}/c)^2$ for charged pions in 12.2 GeV/c p-p collisions. In the work of Akerlof *et al.*[17] the transverse momentum is measured at a fixed value of the longitudinal momentum ($P_L = 0.6$ GeV/c), whereas in this paper the P_T^2 distribution is given for all values of longitudinal momenta. We have also distinguished between the pions produced in the forward and backward hemispheres. The experiments of Ratner *et al.*[18] give a sharp forward peak $[\exp(-10P_T^2)]$ for low-P_T^2 values of positive pions in 500, 1100, and 1500 GeV/c p-p collisions.

The transverse-momentum distributions for the secondary positive pions produced in the forward and backward hemispheres in the reaction $\pi^-\text{CNO} \rightarrow \pi^+ +$ anything are shown in Fig. 2. In Figs. 2(a) and 2(b), the target mass is taken to be equal to the average value of CNO mass for calculating the value of γ_c in order to distinguish the secondary pion, whether it is in the forward hemisphere or in the backward hemisphere. In Figs. 2(c) and 2(d), the target is taken as a proton for calculating γ_c. Similarly, Fig. 3 shows the transverse-momentum distributions for the negative pions produced in the reaction $\pi^-\text{CNO} \rightarrow \pi^-$ + anything, for forward and backward hemispheres and for target mass taken as the average of CNO mass and proton mass. In each case, there is a sharp peak and a shallow one. The values of the slopes are given in Table I. The solid lines represent the best fits to the data.

In the forward hemispheres, comparing the distributions in Figs. 2(b)–2(d) in the case of positive pions and in Figs. 3(b)–3(d) in the case of negative pions, we find that the form of the distributions are exactly the same. This means that the basic features of nucleon-nucleus interactions are nearly similar to those of nucleon-nucleus interactions. This result can also be understood from the fact that at high energies the Lorentz factor does not change appreciably from the primary collision to the secondary collisions, as all these collisions involve low momentum transfer (soft collision). Baroni *et al.*[19] have calculated correlation functions in proton-nucleus interactions at 300 GeV/c assuming the target as a proton. All these factors show that we are justified in considering the target nucleus as a nucleon for calculating the Lorentz factor γ_c. Moreover, considering the nucleon-nucleus interactions from a "microscopic" point of view according to the Field and Feynman[20] picture, one valence quark from the projectile scatters elastically from only one valence quark in the target. If this were not so, there would be a cascade of secondary particles for exceeding the observed experimental multiplicity in such interactions.

Figures 4 and 5 show the transverse-momentum distributions for positive and negative secondary pions in forward and backward hemispheres in the π^-AgBr interactions. For calculating the Lorentz factor γ_c, the distributions are drawn for two cases, (i) where target mass is equal to the average of AgBr mass and (ii) where target mass is equal to proton mass. As in the CNO case it is found here also after comparing the distributions in Figs. 4(b)–4(d) in the case of positive pions and in Figs. 5(b)–5(d) for negative pions that the form of the distributions remains the same even when the AgBr mass is replaced by proton mass. In each case, there is a sharp slope and a shallow one, the

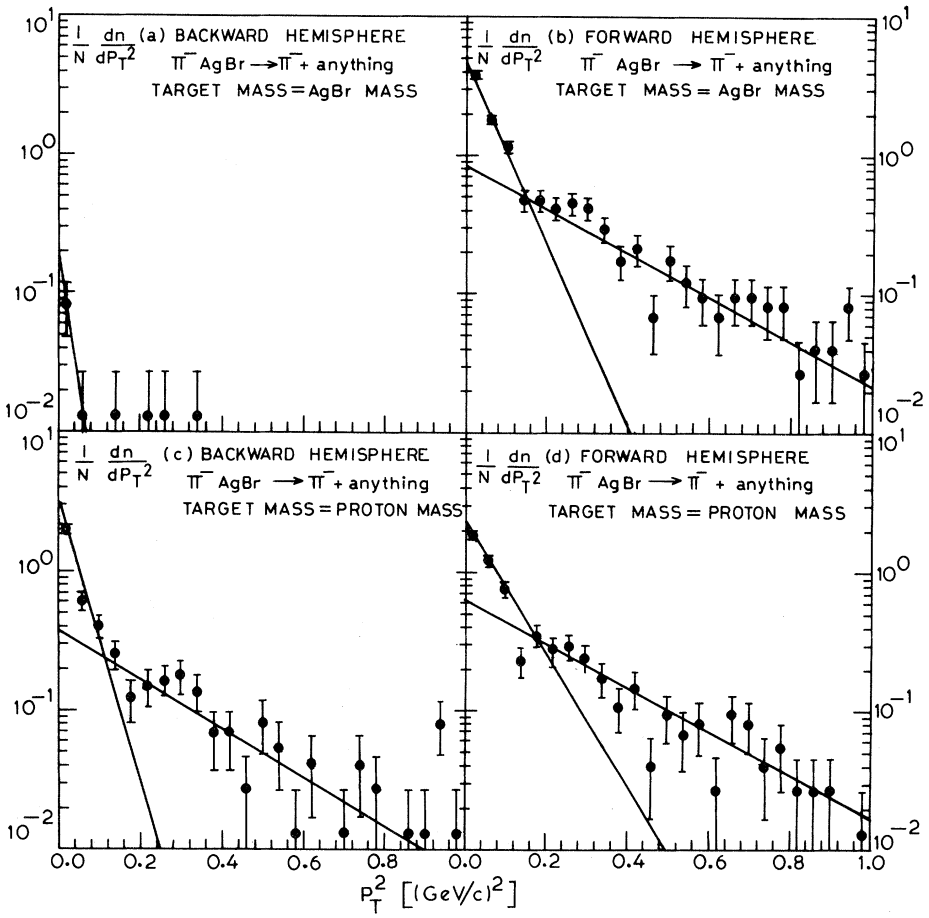

FIG. 5. $P_T{}^2$ distributions of negative secondary pions in (a) and (c) backward and (b) and (d) forward hemispheres in π^-AgBr interactions. In (a) and (b) the target mass is equal to AgBr mass whereas in (c) and (d) the target mass has been taken equal to proton mass. The forms of the solid lines which represent best fits to the data are described in the text and their values are given in Table I.

values of which are given in Table I. The solid lines represent the best fits to the data. Thus, nucleon-nucleus interactions behave essentially as nucleon-nucleon type of interactions.

Yen and Berger[1] have explained the sharp forward peak in the P_T distributions of hadrons as due to the decay of peripherally produced nucleon resonances. The peak in the low-P_T region is due

TABLE II. Various valence quark distributions and the total valence-quark momentum in the pion are shown. Field-Feynman and Dao *et al.* distributions are from Refs. 20 and 23, respectively. The sea quark distribution is of the form $F_s = A(1-x_1)^N$ from which various values of A are calculated for different N applying the given constraint on total sea momentum.

Valence quark distribution in pion $F_v(x_1)$	Total valence-quark momentum f_v	Constraint on total sea-quark momentum f_s	A for $N=5$	A for $N=6$	A for $N=7$	A for $N=8$
$(\frac{3}{4})\sqrt{x_1}(1-x_1)$	0.40	0.60	0.90	1.05	1.20	1.35
$(\frac{15}{16})\sqrt{x_1}(1-x_1)^2$	0.29	0.71	1.07	1.25	1.43	1.61
Field-Feynman (Ref. 20)	0.32	0.68	1.02	1.19	1.36	1.53
Dao *et al.* (Ref. 23)	0.42	0.58	0.87	1.02	1.16	1.31

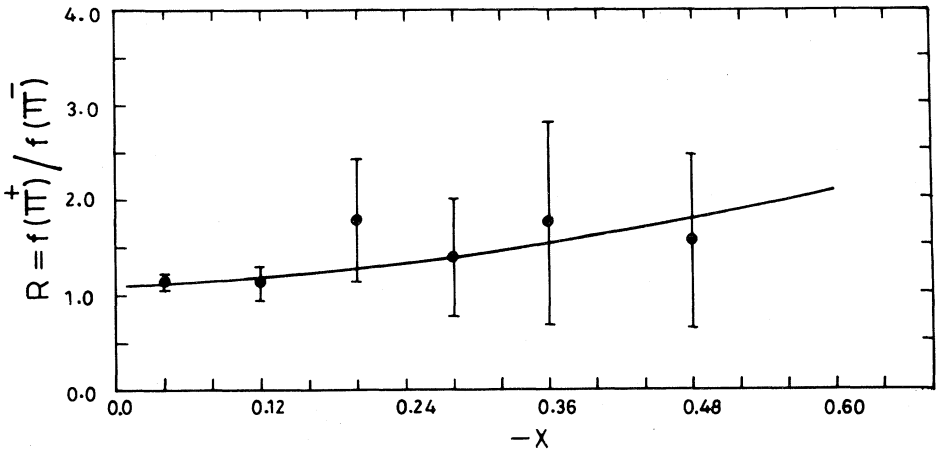

FIG. 6. The π^+/π^- ratio R as a function of $-x$ in the emulsion (backward hemisphere) in π^- interactions with the average mass of emulsion nuclei. The solid curve represents the model prediction discussed in the text.

to the small Q values of the resonances and the large ratio of resonance mass to pion mass. Recently, Whitmore has also explained the $P_T{}^2$ spectra of π, K_s^0, and Λ^0 by assuming them to be the decay products of ρ^0, $K^*(890)$, and $\Sigma(1385)$ using the Monte Carlo simulation technique.[21] The impressive agreement with the experiment shows the strong contribution of resonances. We find a peak in the low-P_T region not only for forward pions but also for backward pions. This has been observed for both positive and negative pions. In the present interactions, the nucleon resonances are probably produced both in the forward as well as in the backward directions. It would be quite interesting to verify if the low-P_T distribution of pions produced in different targets at different primary energies can also be described by the above approach.

B. Recombination model in the central region

The secondary hadrons (pions) can be produced via two processes: (a) A scattered valence quark (antiquark) may pick up an antiquark (quark) from the sea or (b) the quarks and antiquarks from the sea alone may recombine to produce a hadron. The possibility of valence quarks fragmenting into more valence quarks and then being available for recombination among themselves or with sea quarks is discounted, because at low transverse momentum $P_T \leq 1$ GeV/c) and in the low-x region ($x \leq 0.5$) for which our data is available, the collision is "soft" and hence practically no valence fragmentation takes place. Valence fragmentation takes place in "hard" processes only. Das and Hwa[3] have shown that valence-quark fragmentation cannot contribute more than about 1% of the

TABLE III. Values of χ^2/DOF for N in π^-N, π^-CNO, and π^-AgBr interactions, for various distributions obtained from different valence quark distributions and sea quark distributions as prescribed in relation (2) in the text. Field-Feynman and Dao *et al.* distributions are from Refs. 20 and 23, respectively.

Valence and sea distributions in the pion Reaction	$\frac{3}{4}\sqrt{x_1}(1-x_1)$ and $F_s(x_1)=A(1-x_1)^N$ N	χ^2/DOF	$\frac{15}{16}\sqrt{x_1}(1-x_1)^2$ and $F_s(x_1)=A(1-x_1)^N$ N	χ^2/DOF	Field-Feynman and $F_s(x_1)=A(1-x_1)^N$ N	χ^2/DOF	Dao *et al.* and $F_s(x_1)=A(1-x_1)^N$ N	χ^2/DOF
π^-N	5	2.546/5	5	1.792/5	6	1.395/5	5	3.733/5
π^-CNO	5	3.213/6	5	2.616/6	6	2.361/6	5	4.149/6
π^-AgBr	8	6.736/5	8	6.091/5	8	6.013/5	7	7.227/5

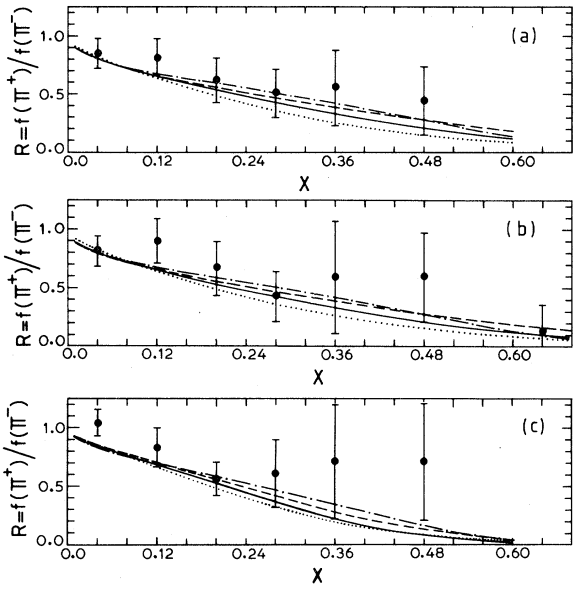

FIG. 7. The π^+/π^- ratio R as a function of x in the pion (forward hemisphere) in (a) π^-N, (b) π^-CNO, and (c) π^-AgBr interactions. The distributions represented by solid, dashed, dash-dot, and dotted curves are obtained as prescribed in relation (2) in the text by the combination of sea quark distribution of the form $F_s=A(1-x_1)^N$ to each of the valence quark distributions of the form $(\frac{3}{4})\sqrt{x_1}(1-x_1)$, $(\frac{15}{16})\sqrt{x_1}(1-x_1)^2$, Field-Feynman and Dao *et al.*, respectively. The values of N for these distributions are given in Table III.

single-meson production cross section at low P_T and large x ($0.5 \leq x \leq 1.0$). Therefore, at low x ($x \leq 0.5$) the valence fragmentation contribution to meson production will be even lower than 1%, which can be neglected. Hence, the meson production in the low-x region ($x \leq 0.5$) is predominately from the recombination of quarks and antiquarks in the sea. The gluons also create quark-antiquark pairs in the sea which eventually convert to mesons. This is supported by Van Hove,[7] who has suggested that in high-energy collisions of the low-P_T type, valence quarks, which retain their original fraction x of incident momentum, hadronize by recombining with each other and/or with additional low-x partons from the sea. Hadrons produced in this way are in the fragmentation regions, i.e., regions of medium and high x of either sign. In the central region (low-x region), hadronization is mainly from the excited gluon sea.

In the model of Das and Hwa,[3] the Feynman-x distribution of single-meson production is given by

$$f(x)=\frac{Ed\sigma}{\sigma_T dp_L} = \frac{c(1-x)}{x}\int_0^x F_q(x_1)F_{\bar{q}}(x-x_1)dx_1 , \tag{1}$$

where $F_q(x_1)$ and $F_{\bar{q}}(x_1)$ are the x distribution functions of the quarks and antiquarks, respectively, in the incident hadron, and c is the phase-space factor which is only approximately correct since several approximations are involved in its calculation. In our analysis we are only considering particle production ratios where this phase-space factor c cancels out. The π^+/π^- ratio R is given by the ratio of the integrals

$$R=\frac{f(\pi^+)}{f(\pi^-)} = \frac{\int_0^x F_u(x_1)F_{\bar{d}}(x-x_1)dx_1}{\int_0^x F_d(x_1)F_{\bar{u}}(x-x_1)dx_1} . \tag{2}$$

Hence for a steeply falling sea distribution in a

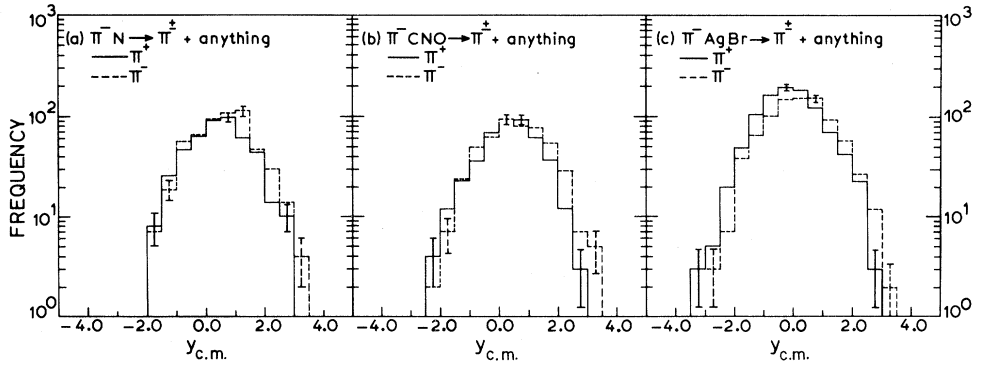

FIG. 8. Single-particle inclusive rapidity distributions of secondary pions produced in (a) π^-N, (b) π^-CNO, and (c) π^-AgBr interactions, respectively. The solid line represents the positive pion distribution and the dashed line represents the negative pion distribution.

proton, the ratio of these integrals become approximately $\sim F_u(x)F_d(0)/F_d(x)F_{\bar{u}}(0) \sim u(x)/d(x)$, which is consistent with the observation of Ochs.[22]

In the backward hemisphere, we followed Duke and Taylor[4] in determining the distribution functions. For the functions $F_u(x)=xu(x)$ and $F_d(x)=xd(x)$, we used the Field and Feynman[20] valence quark distributions plus the sea quark distributions of Duke and Taylor.[4] This has been achieved by subtracting the Field-Feynman sea distributions from their fits to $xu(x)$ and $xd(x)$ and adding the sea distributions of Duke and Taylor. All the sea quark (u, $\bar{u}$, d, and $\bar{d}$) distributions are of the form $F_{\text{sea}}(x_1)=q_s(1-x_1)^n$, as determined by Duke and Taylor in p-p collisions. Also, the momentum fraction carried by the various partons in the proton in our case is taken to be the same. Although our target is composed of emulsion nuclei and not of protons only, even then these valence and sea distributions explain the π^+/π^- ratio very well.

In the forward hemisphere (that is, in the pion fragmentation region) we followed the work of Biswas *et al.*[5] in evaluating the valence and sea quark distribution functions. As the valence quark (antiquark) distributions in the pion are not well determined, we assume four different forms of the valence distribution functions (Table II). The first two forms have been suggested by Biswas *et al.*[5] The third distribution represents the Field and Feynman[20] parametrization for the pion valence quark distributions, which approaches a constant value at large x_1. Dao *et al.*[23] have calculated the pion valence quark distributions for dimuon production in π-p interactions assuming a Drell-Yan process, which has been considered as the fourth function. Each assumed valence quark distribution is normalized so that

$$\int_0^1 [F_v(x_1)/x_1]dx_1=1 ,$$

and the total momentum fraction f_v carried by the valence quarks is given by $2\int_0^1 F_v(x_1)dx_1$. The details of the valence quark distributions and the total valence momentum fractions f_v are given in Table II. The distributions for each of the sea quarks and antiquarks (d, $\bar{d}$, u, $\bar{u}$) in our analysis is assumed to be of the form $F_s=A(1-x_1)^N$. For determining the π^+/π^- ratio R as a function of Feynman x, the ratio of integrals in relation (2) is evaluated using the aforementioned sea and valence quark (antiquark) distributions. Since there is practically no valence fragmentation in low-P_T region ($P_T \leq 1$ GeV/c) according to Das and Hwa, the positive pions in the forward hemisphere (pion fragmentation region) will come from the recombination of quarks and antiquarks from the sea only, whereas the secondary negative pions will have the contribution of two valence quarks (d and $\bar{u}$) from the incident π^-. Therefore, in relation (2), both the functions F_u and $F_{\bar{d}}$ in the numerator are of the form $F_s=A(1-x_1)^N$, whereas in the denominator one is the sea quark function and the other is one of the four assumed valence quark functions. Both A and N are varied to obtain the best fits to the data for the π^+/π^- ratio R. However, A and N are not determined arbitrarily, but are evaluated according to the momentum sum rule. The momentum fraction carried by the sea quarks is $\leq 1-f_v$, as the momentum fraction attributed to valence quarks is f_v. Neglecting the insignificant momentum contribution of strange sea quarks in the pion, we have the momentum constraint that

TABLE IV. Values of χ^2/DOF for single- and double-exponential distributions for different types of inclusive interactions.

Distribution type	$dn/dr=Ae^{-Br}$			$dn/dr=Ae^{-Br}+Ce^{-Dr}$				
	A	B	χ^2/DOF	A	B	C	D	χ^2/DOF
$\pi^-N\to\pi^+\pi^-$ + anything	2.1±1.0	2.2±0.1	20.8/24	1.9±1.0	2.2±0.2	0.2±0.2	2.1±0.4	20.8/24
$\pi^-N\to\pi^+\pi^+$ + anything	1.8±1.1	1.8±0.2	8.9/19	1.4±1.2	1.8±0.6	0.4±0.5	1.9±0.6	8.9/19
$\pi^-N\to\pi^-\pi^-$ + anything	2.0±1.1	2.1±0.2	20.2/20	2.1±1.2	3.0±0.7	0.15±0.4	0.2±0.8	16.0/20
π^-CNO$\to\pi^+\pi^-$ + anything	2.2±1.1	2.4±0.2	24.1/24	1.4±1.5	3.1±1.2	0.9±0.9	1.9±0.9	23.7/24
π^-CNO$\to\pi^+\pi^+$ + anything	1.9±1.1	2.1±0.2	16.8/20	2.0±1.2	2.7±0.7	0.1±0.2	0.1±0.7	15.5/20
π^-CNO$\to\pi^-\pi^-$ + anything	1.9±1.0	2.0±0.1	8.8/22	2.0±1.2	3.0±0.6	0.2±0.3	0.4±0.4	5.7/22
π^-AgBr$\to\pi^+\pi^-$ + anything	2.3±1.0	2.4±0.1	25.3/24	2.2±1.0	2.4±0.2	0.1±0.4	2.4±0.3	25.3/24
π^-AgBr$\to\pi^+\pi^+$ + anything	2.5±1.0	2.6±0.1	16.3/23	2.5±1.1	2.9±0.3	0.1±0.4	0.7±0.3	14.8/23
π^-AgBr$\to\pi^-\pi^-$ + anything	2.4±1.1	2.7±0.2	30.8/22	2.5±1.3	3.4±0.7	0.15±0.5	0.6±0.6	27.9/22

$$f_s = 4\int_0^1 F_s(x_1)dx_1 = 4A/(N+1)\,. \quad (3)$$

The values of the constraint on total sea momentum f_s and A for $N=5$, 6, 7, and 8 are given in Table II for different valence distributions.

Following the above-mentioned procedure, we evaluated the valence and sea quark distributions in the pion in $\pi^- N$, π^-CNO, and π^-AgBr interactions. The valence and sea quark distributions have also been evaluated in the target in the backward hemisphere taking the average mass of the emulsion nuclei which is ~ 73.

Effects of resonances in secondary pion distributions in the proton fragmentation region has been studied by Roberts, Hwa, and Matsuda.[24] They observe that the model of Das and Hwa[3] is still applicable if the contribution of resonances is taken into account. Biswas *et al.*[5] have studied their distributions in two different ways, (a) by neglecting resonance production and (b) by subtracting the estimated resonance contribution to inclusive pion distributions. They find that their valence plus sea

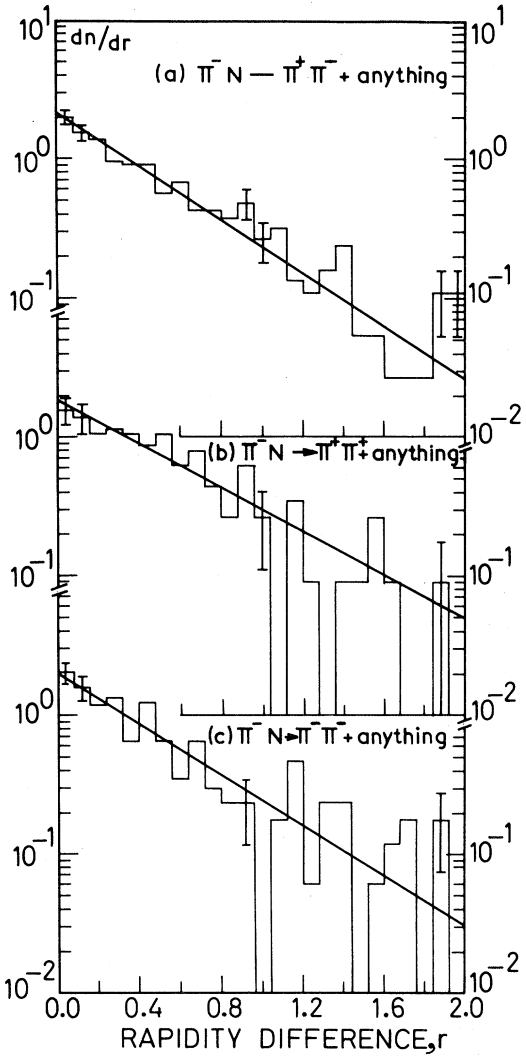

FIG. 9. Rapidity-difference (r) distributions of charged secondary particles produced in $\pi^- N$ interactions for (a) $\pi^+\pi^-$, (b) $\pi^+\pi^+$, and (c) $\pi^-\pi^-$ adjacent pions in ordered rapidity space. The solid curves in (a), (b), and (c) are the predictions of single exponential distributions given in Table IV.

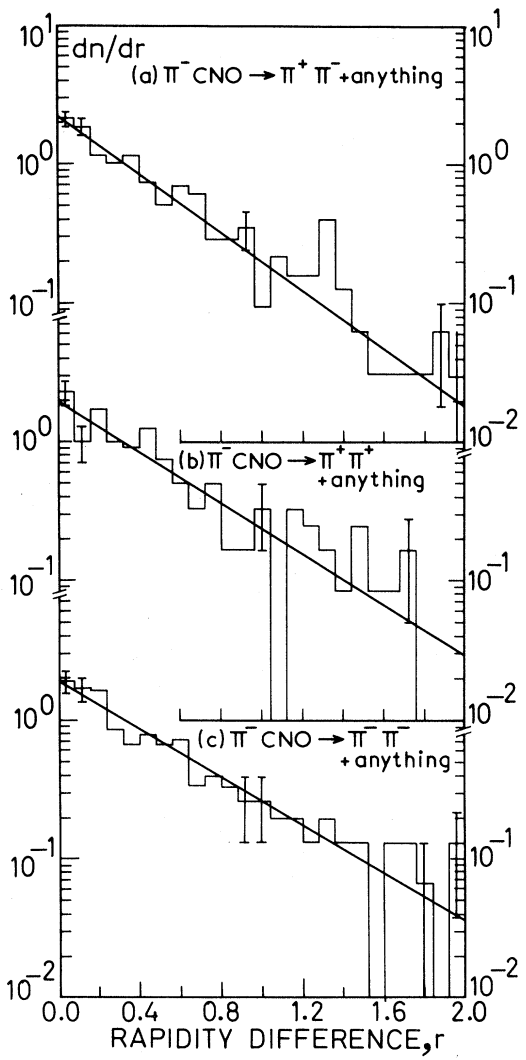

FIG. 10. Rapidity-difference (r) distributions of charged secondary particles produced in π^-CNO interactions for (a) $\pi^+\pi^-$, (b) $\pi^+\pi^+$, and (c) $\pi^-\pi^-$ adjacent pions in ordered rapidity space. The solid curves in (a), (b), and (c) are the predictions of single-exponential distributions given in Table IV.

quark distributions obtained from the model fall somewhat below the experimental points in the former case. According to Duke and Taylor, if the resonances, which contribute more strongly to the π^+/π^- ratio at small x, are taken into account, then only the magnitudes and shapes determined for the sea distributions will change. In other words, this is supported by Van Hove,[7] who has suggested that the hadrons produced in the central region (low-x region) mainly result from hadronization of the excited gluon sea. This means that resonances in the low-x region come from the excited gluon sea, thereby changing only the magnitudes of the sea distributions and not the form which remains as $F_s = A(1-x_1)^N$. Considering these factors, we have not subtracted the resonance contribution to the pion distributions, and have evaluated the sea distributions for the low-x region ($x \leq 0.5$) for which our data is available. Again, we are justified in considering the whole of the low-x region ($0.0 \leq x \leq 0.5$) for the reasons given above.

Figure 6 shows the experimental distribution of the π^+/π^- ratio R as a function of x in the backward hemisphere. The secondary pions considered here are produced from all the nuclei of the emulsion at small x ($x \leq 0.5$). Values of R have been combined for all the emulsion nuclei in order to augment the statistics. Hence, in this target fragmentation region we are studying the π^+/π^- ratio for the average mass of all the emulsion nuclei. This ratio can be well explained on the basis of the recombination model. The solid line in Fig. 6 represents the theoretical distribution obtained following the method adopted by Duke and Taylor.[4] The sea distribution which gives the best fit to the data in our case is $F_s = 0.80(1-x_1)$.[5] The momentum fraction carried by various partons remains the same as in the case of Duke and Taylor. The χ^2/DOF for the distribution is 0.998/5, which gives a fairly good confidence level. It can be concluded here that the various valence (u,d) and sea $(\bar{u},\bar{d})$ distributions in proton obtained by Duke and Taylor can also be successfully applied to explain the secondary pion production from the larger emulsion nuclei.

The π^+/π^- ratios R as a function of x in the forward hemisphere (pion fragmentation region) in π^-N, π^-CNO, and π^-AgBr interactions are given in Figs. 7(a)–7(c), respectively. In Fig. 7(a), we fitted the four different distributions obtained from each of the four different forms of valence quark distributions combined with the sea distribution of the form $A(1-x_1)^N$ to the π^+/π^- data in π^-N interactions as prescribed by relation (2). The details of the valence and sea quark distributions are given in Table II. The value of N and consequently of A is varied to obtain the best fit. The magnitudes of A for different values of N which saturate the momentum sum rule in various distributions are also shown in Table II. The values of N thus obtained from the best fits and the values of χ^2 and χ^2/DOF for each distribution are given in Table III. The various lines in the figure represent the best fits to the data for which the χ^2 values are

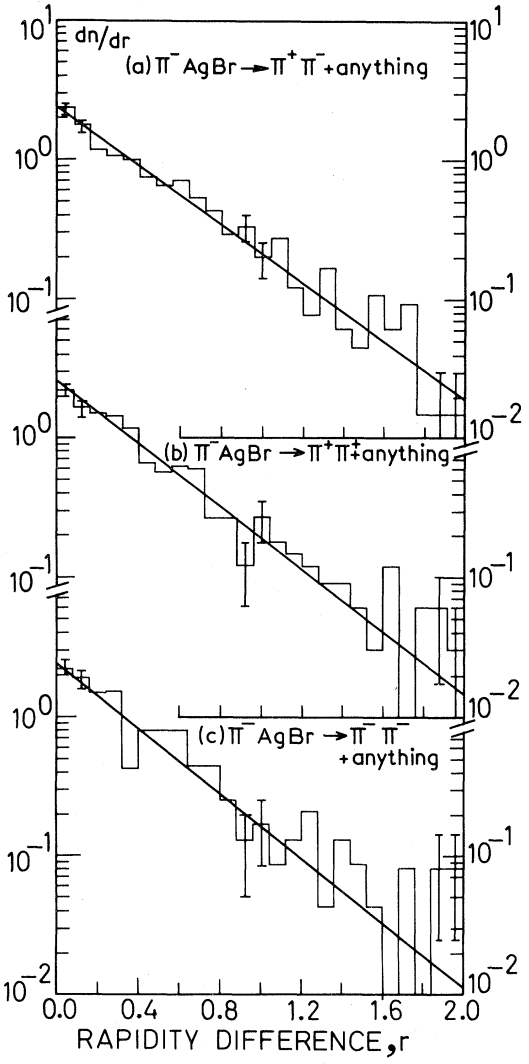

FIG. 11. Rapidity-difference (r) distributions of charged secondary particles produced in π^-AgBr interactions for (a) $\pi^+\pi^-$, (b) $\pi^+\pi^+$, and (c) $\pi^-\pi^-$ adjacent pions in ordered rapidity space. The solid curves in (a), (b), and (c) are the predictions of single-exponential distributions given in Table IV.

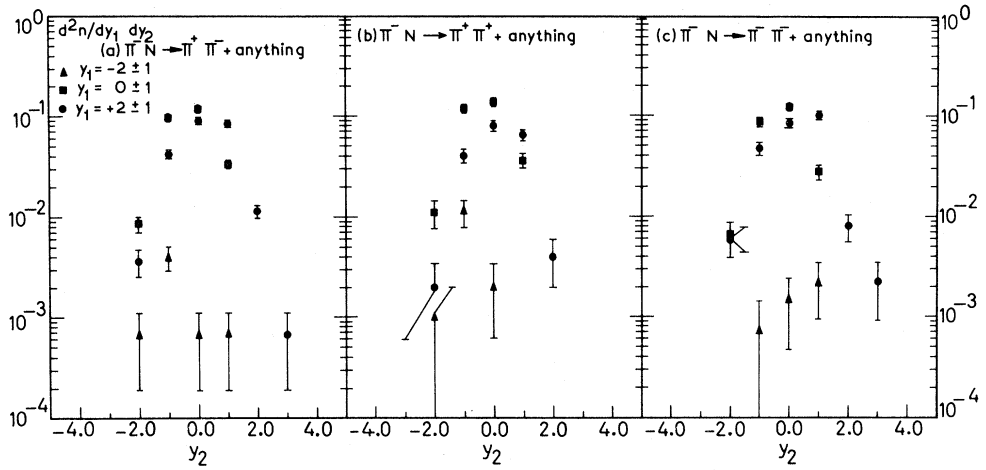

FIG. 12. Two-particle inclusive rapidity distributions in the c.m. system for all combinations of secondary pions produced in interactions (a) $\pi^- N \to \pi^+ \pi^-$ + anything, (b) $\pi^- N \to \pi^+ \pi^+$ + anything, and (c) $\pi^- N \to \pi^- \pi^-$ + anything, as a function of single-particle rapidities.

the lowest. Similarly, we obtained the best fits to π^+/π^- data in the pion in π^-CNO and π^-AgBr interactions which are shown in Figs. 7(b) and 7(c), respectively. The values of N obtained from the best fits and values of χ^2 and χ^2/DOF for each distribution in these cases are also given in Table III. It is evident from the χ^2/DOF values that all the theoretical fits to the data have a fairly good confidence level.

The value of N is 5 or 6 in $\pi^- N$ interactions as well as in π^-CNO interactions, but it increases to 7 or 8 in the case of π^-AgBr interactions when we consider different model parametrizations as prescribed by relation (2) (Table III). This can be explained as follows. The interaction time increases with the increase in target size, because the valence quarks of the projectile have to traverse a longer distance in the larger nucleus. A larger number of quark-antiquark pairs are produced in the sea because of the longer time available. These quarks and antiquarks recombine to produce secondary mesons, thereby giving higher multiplicity in hadron-nucleus interactions. Now as the total momentum fraction of sea quarks f_s is constant in hadron-hadron and hadron-nucleus interactions, this fraction of momentum is distributed among a larger number of sea quarks reducing the individual share of momentum of each sea quark to very small values. Therefore in hadron-nucleus interactions the sea distribution will fall sharply with an

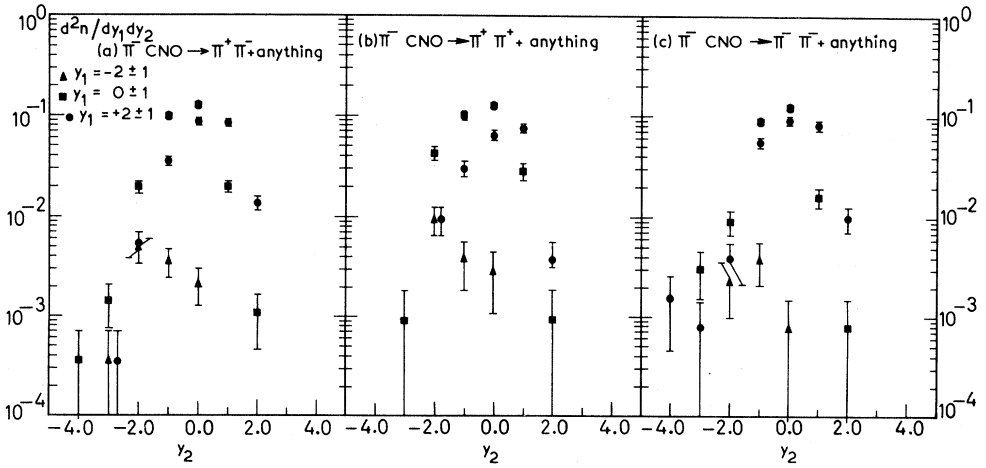

FIG. 13. Two-particle inclusive rapidity distributions in the c.m. system for all combinations of secondary pions produced in interactions (a) π^-CNO$\to\pi^+\pi^-$ + anything, (b) π^-CNO$\to\pi^+\pi^+$ + anything, and (c) π^-CNO$\to\pi^-\pi^-$ + anything, as a function of single-particle rapidities.

increase in x. Hence, we can conclude that the value of N is directly proportional to the number of sea quarks produced in an interaction.

It can be seen from Table III that each of the four distributions obtained from various valence distributions combined with sea distributions give a good description of the data. Since the difference among the four model predictions is very small, it would need high statistics to establish a sharp distinction between the various models. Our low-event statistics forbids us to achieve this purpose. It would, however, be interesting to study the sea and valence quark distributions in nuclear targets and make a comparative study of the models in a high-statistics experiment.

C. Correlations among secondary particles

In this paper, in order to display the inclusive distributions we choose the rapidity variable

$$Y=\frac{1}{2}\ln\left[\frac{E+P_L}{E-P_L}\right], \tag{4}$$

where E and P_L are the energy and the longitudinal momentum of the secondary pion. The two-particle normalized correlation function is usually defined as

$$R(Y_1,Y_2)=\frac{\sigma_{\text{in}}d^2\sigma/dy_1dy_2}{(d\sigma/dy_1)(d\sigma/dy_2)}-1, \tag{5}$$

$$=\frac{N_TN_2(Y_1,Y_2)}{N_1(Y_1)N_1(Y_2)}-1, \tag{6}$$

where N_T is the total number of inelastic events in a particular interaction, $N_2(Y_1,Y_2)$ is the number of pairs of tracks with rapidities Y_1 and Y_2, and $N_1(Y_1)$ and $N_1(Y_2)$ are the number of secondary particles with c.m. rapidities Y_1 and Y_2, respectively.

Figure 8 shows the single-particle inclusive rapidity distributions of secondary pions produced in three types of interactions, namely, (a) π^-N, (b) π^-CNO, and (c) π^-AgBr interactions, respectively. The solid line shows the positive-pion distribution whereas the dashed line shows the negative-pion distribution. The distributions in all the three cases are narrow and sharply peaked, lacking a plateau in the central region. This is so, because no correlations are evident among these secondary pions. The narrowness of the distributions is expected due to the low primary energy. It is seen that in all three cases the negative-pion distribution is slightly shifted toward higher values of rapidity than the positive-pion distribution. This may be because of the contribution of the incident negative pions which have not been taken out of the data. From Fig. 8, it is evident that the peak of the distributions shifts toward lower values of rapidity with the increase in target size. Also, an increasing percentage of secondary pions populate the lower values of rapidity, that is in the backward hemisphere, with the increase in target size. These results are in agreement with the model of Capella and Krzywicki.[25] They suggest that dN^{hA}/dY increases appreciably with $\bar{\nu}$ in the central region as well as in the fragmentation region of the nucleus, where $\bar{\nu}$ is the average number of subcollisions and

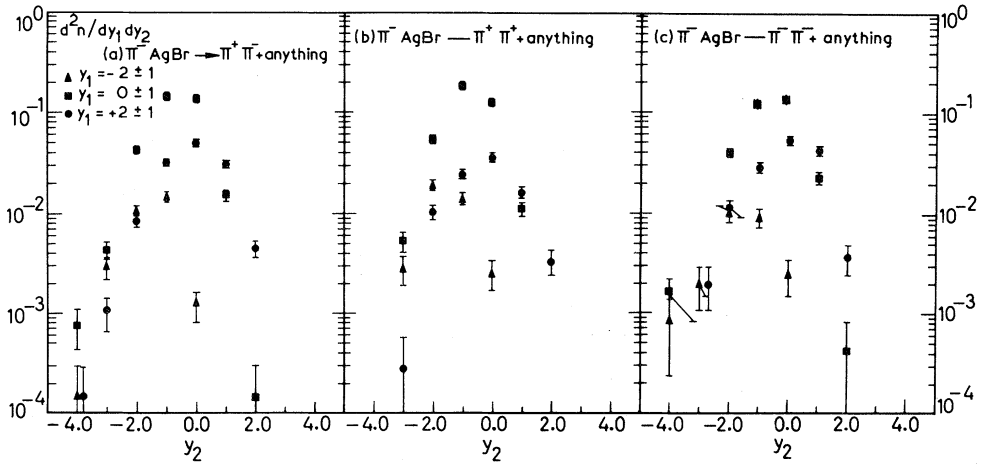

FIG. 14. Two-particle inclusive rapidity distributions in the c.m. system for all combinations of secondary pions produced in interactions (a) π^-AgBr→$\pi^+\pi^-$ + anything, (b) π^-AgBr→$\pi^+\pi^+$ + anything, and (c) π^-AgBr→$\pi^-\pi^-$ + anything, as a function of single-particle rapidities.

can be regarded as effective target mass. The $\bar{\nu}$ dependence is negligible in the fragmentation region of the projectile. The maxima of the rapidity distribution moves toward smaller values of rapidities with an increase in $\bar{\nu}$. This is because the average energy of a subcollision is decreasing with an increase in the average multiplicity which is proportional to $\bar{\nu}$. Thus we find that all these features which are present in our data can be explained well on the basis of this model.

It has been shown[26] that the existence of correlations can be determined by means of rapidity-difference distributions. In another paper[9] we suggested a model-independent method of determining the strength of correlation and cluster size and its dependence on primary energy. If there is independent emission of secondary pions and hence absence of correlations, the rapidity distribution will be narrow and a sharply peaked one. The rapidity-difference distribution for such pions can be explained by the single exponential distribution of the form

$$dn/dr = Ae^{-Br} . \tag{7}$$

This view is supported by Quigg, Pirila, and Tho-

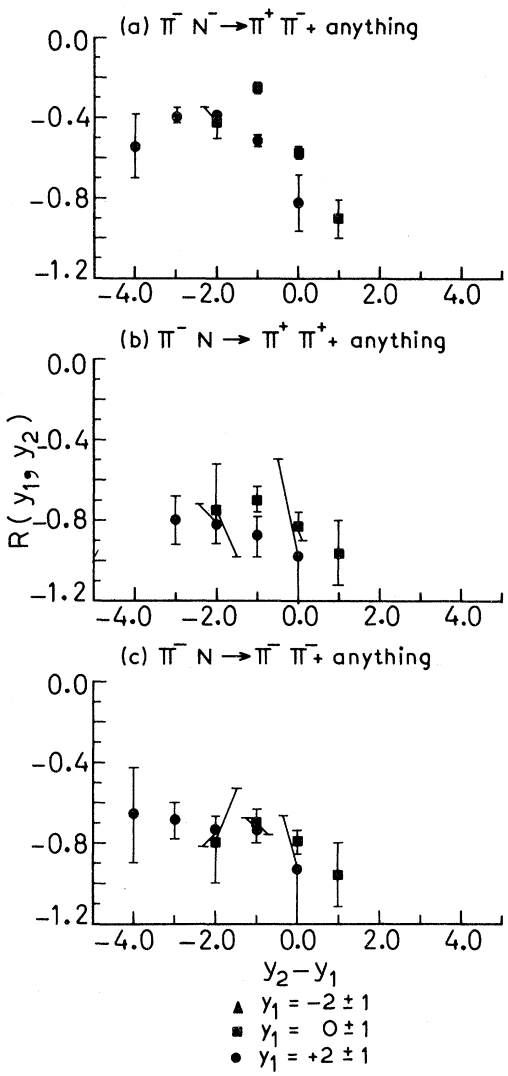

FIG. 15. The two-particle correlation function R plotted as a function of the difference between the rapidities of the two pions in the reactions (a) $\pi^- N \rightarrow \pi^+\pi^- +$ anything, (b) $\pi^- N \rightarrow \pi^+\pi^+ +$ anything, and (c) $\pi^- N \rightarrow \pi^-\pi^- +$ anything.

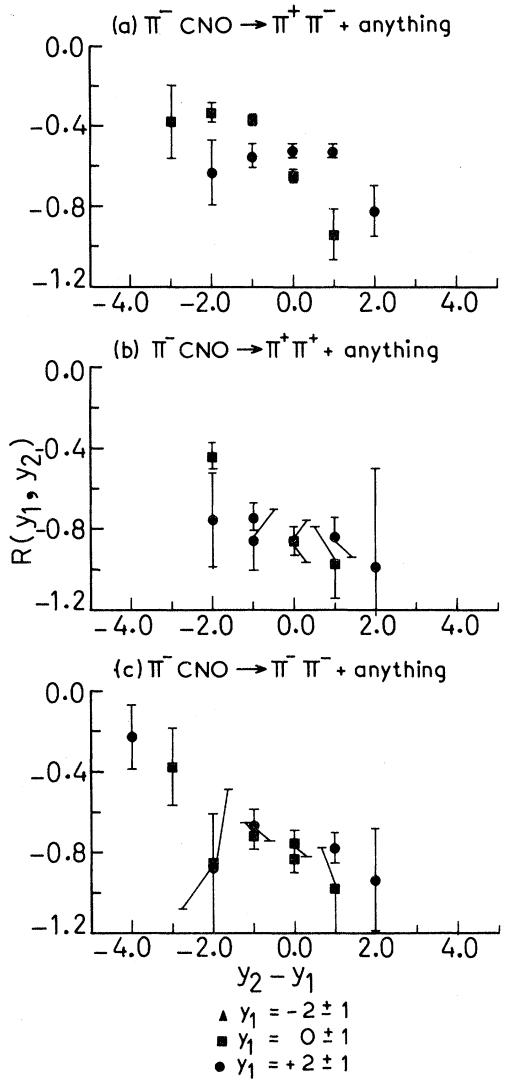

FIG. 16. The two-particle correlation function R plotted as a function of the difference between the rapidities of the two pions in the reactions (a) π^-CNO $\rightarrow \pi^+\pi^- +$ anything, (b) π^-CNO$\rightarrow \pi^+\pi^+ +$ anything, and (c) π^-CNO$\rightarrow \pi^-\pi^- +$ anything.

mas[27] who have suggested that a single exponential behavior of the rapidity-difference distribution establishes the production of uncorrelated particles, preferably with large gaps (r). Deviations from the exponential behavior at small rapidity gaps demonstrates the existence of short-range positive correlations. If a double-exponential distribution of the form

$$dn/dr = Ae^{-Br} + Ce^{-Dr} \tag{8}$$

fits the data well, this would mean that there is production of correlated particles from the decay of clusters (explained by the first exponential term) over and above the background of independently emitted particles described by the second term. Thus a sharp peak at small values of the rapidity difference indicating strong two-particle correlation can be understood. This behavior is also in agreement with the multiperipheral model proposed by Snider[28] in which the secondary particles are the decay products of the clusters formed at the vertices in a multipheripheral chain.

In order to determine the best theoretical curve which would fit the observed rapidity-difference distributions, single- and double-exponential distributions were tried using an IBM 360 computer. Various values of the parameters were tried in the equations. It was found that both the equations yielded nearly the same value of χ^2. The method adopted for calculating χ^2 values is the same as followed in an earlier work[15] in which dependence of cluster size and strength of correlation on inelasticity in cosmic-ray interactions was studied. The value of χ^2 and χ^2/DOF for single- and double-exponential curves for different distributions are given in Table IV.

Figure 9 shows the two-particle rapidity-difference (r) distributions of adjacent secondary pions, ordered in rapidity space produced in $\pi^- N$ interactions. Figure 9(a) shows the rapidity-difference distribution of adjacent $\pi^+\pi^-$ combination. Figures 9(b) and 9(c) show the distributions for adjacent $\pi^+\pi^+$ and $\pi^-\pi^-$ combinations, respectively. It is clear from Table IV, that both single-exponential distributions and double-exponential distributions for these three cases yield approximately the same value of χ^2/DOF. Hence it can be concluded that no correlations are evident at the level of statistics of the present experiment.

Following the same procedure, the two-particle rapidity-difference distributions were calculated for adjacent combinations of $\pi^+\pi^-$, $\pi^+\pi^+$, and $\pi^-\pi^-$ in π^-CNO and π^-AgBr interactions and are shown in Figs. 10 and 11, respectively. The curves represented by the solid lines are the predictions of the single-exponential distribution whose parameters are given in Table IV. It is evident that the single-exponential distributions can well explain the behavior of particle production in all the cases. Hence, it can be concluded that no correlations are evident at the level of statistics of the present experiment.

Two-particle rapidity distributions and normalized correlation function R have been used by various investigators[29] to study the existence of short-

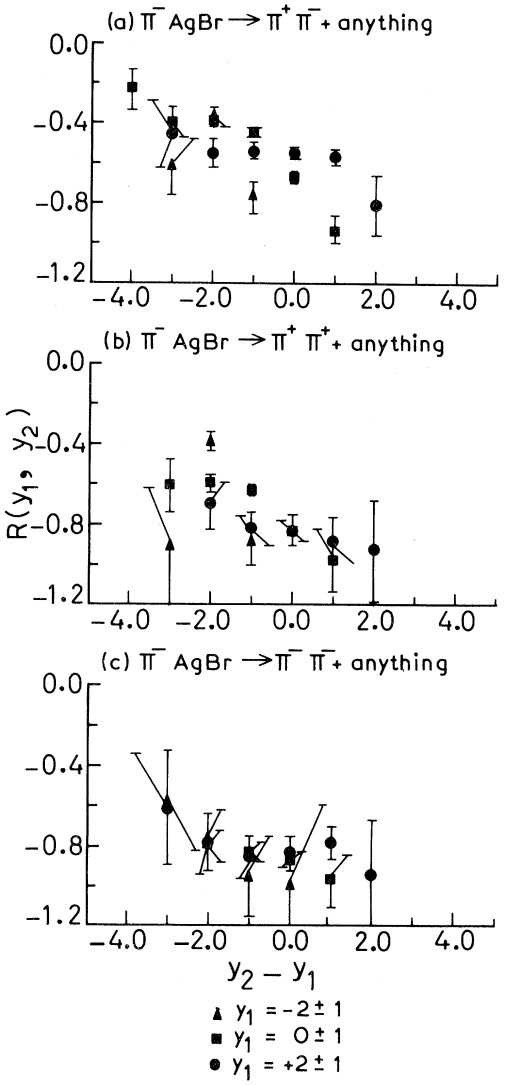

FIG. 17. The two-particle correlation function R plotted as a function of the difference between the rapidities of the two pions in the reactions (a) π^-AgBr $\rightarrow\pi^+\pi^-$ + anything, (b) π^-AgBr $\rightarrow\pi^+\pi^+$ + anything, and (c) π^-AgBr $\rightarrow\pi^-\pi^-$ + anything.

range positive correlations among secondary hadrons in high-energy interactions. Following this alternative approach we investigated the existence of correlations in these interactions. Figures 12(a)—12(c) show the two-particle inclusive rapidity distribution for particle combinations of $\pi^+\pi^-$, $\pi^+\pi^+$, and $\pi^-\pi^-$, respectively. It is observed that $d^2n/dY_1\,dY_2$ peaks around $Y_2-Y_1\approx 0$. The shapes of these two-particle distributions are not any narrower than that of the single-particle rapidity distributions, thus signifying the absence of correlations. In Figs. 13 and 14 are shown two-particle rapidity distributions of secondary pions produced in π^-CNO and π^-AgBr interactions, respectively. Here also the shapes of the distributions are similar to their respective single-particle distributions, thus showing the absence of correlations in these interactions. In the case of π^-AgBr interactions the peaking shifts a little backward and is not around $Y_2-Y_1\approx 0$. The explanation for this shift is similar to that for single-particle rapidity distributions discussed earlier.

Next, we study the behavior of the normalized correlation function R as a function of the rapidity separation Y_2-Y_1 for different values of Y_1. In Figs. 15(a)—15(c), we show the correlation function R plotted against Y_2-Y_1 for particle combinations $\pi^+\pi^-$, $\pi^+\pi^+$, and $\pi^-\pi^-$, respectively, for π^-N interactions. Similarly, Figs. 16 and 17 show the plot of correlation function R as a function of rapidity separation Y_2-Y_1 for different values of Y_1 in π^-CNO and π^-AgBr interactions, respectively. The value of R in all the cases is below zero and does not follow any pattern. Thus, no short-range positive correlations are evident in these interactions. It must be remarked that there is an inherent difference between the correlations among the like and unlike pairs of pion. The correlations among unlike charged particles are dynamical in origin but those among like charged particles are due to the Bose-Einstein effect. This has been discussed by Whitmore[30] and Kenney.[31]

Following the three approaches as described above, it is clear that no positive, short-range correlations are evident among the secondary particles produced in light and heavy nuclear targets at a primary energy of 50 GeV/c, at the level of statistics of the present experiment. This result is not totally unexpected. It is in agreement with the earlier work[9] by some of us where we have shown the dependence of strength of correlation on the primary energy. As the primary energy decreases the correlation strength also decreases, reaching a point where it is absent. It has been shown earlier[32] that the strength of correlation increases with multiplicity. Although the average multiplicity in the present interactions is much larger ($=10.7$) for AgBr than for nucleon target ($=5.6$), yet the correlations have not been observed for both types of interactions. This points to the conclusion that it is not the multiplicity but the primary energy that is the dominant criterion for the existence of correlations. The determination of correlations at several energies above 50 GeV/c would enable one to find the value of the primary energy at which correlations set in. This kind of investigation would be interesting in order to understand the dynamics of cluster formation, which would lead to a better understanding of multiparticle production.

[1]E. Yen and E. L. Berger, Phys. Rev. Lett. 24, 695 (1970).
[2]S. Pokoroski and L. Stodolsky, Phys. Lett. 60B, 84 (1975).
[3]K. P. Das and R. C. Hwa, Phys. Lett. 68B, 459 (1977).
[4]D. W. Duke and F. E. Taylor, Phys. Rev. D 17, 1788 (1978).
[5]N. N. Biswas *et al.*, Phys. Rev. D 19, 1960 (1979).
[6]T. A. DeGrand and H. I. Miettinen, Phys. Rev. Lett. 40, 614 (1978).
[7]L. Van Hove, Acta Phys. Austriaca Suppl. 21, 621 (1979); CERN Report No. TH-2628 (unpublished).
[8]Edmond L. Berger, Nucl. Phys. B85, 61 (1975); L. Foa, Phys. Rep. 22C, 1 (1975); R. Slansky, *ibid.* 11C, 99 (1974); J. Whitmore, *ibid.* 27C, 187 (1976); P. Pirila, G. H. Thomas, and C. Quigg, Phys. Rev. D 12, 92 (1975); A. Arneodo and G. Plaut, Nucl. Phys. B107, 262 (1976). Detailed references are given in the above papers.
[9]R. K. Shivpuri and Chandra Gupt, Phys. Rev. D 15, 3332 (1977); R. K. Shivpuri, Chandra Gupt, T. Chand, and T. Singh, *ibid.* 14, 3103 (1976).
[10]I. Hoffman, in Proceedings of the CERN Easter School for Physicists, St. Cergue, 1962 (unpublished), p. 297.
[11]K. D. Tolstov and G. S. Shabratova, Dubna Report No. P1 8402, 1974 (unpublished).
[12]M. Danysz *et al.*, Nucl. Instrum. Methods 24, 103 (1963).
[13]A. Barbaro-Glatieri *et al.*, Nuovo Cimento 21, 469 (1961); B. Bhowmik and R. K. Shivpuri, Phys. Rev.

160, 1227 (1967).
[14]E. M. Friedlander, Nuovo Cimento 14, 796 (1959); A. Barbaro-Galtieri *et al.*, *ibid.* 21, 469 (1961).
[15]Chandra Gupt and R. K. Shivpuri, Phys. Rev. D 19, 2135 (1979).
[16]R. K. Shivpuri and Chandra Gupt, Nuovo Cimento 39, 548 (1977).
[17]C. W. Akerlof *et al.*, Phys. Rev. D 3, 645 (1971).
[18]L. G. Ratner *et al.*, Phys. Rev. D 9, 1135 (1974).
[19]G. Baroni *et al.*, Nucl. Phys. B103, 213 (1976).
[20]R. D. Field and R. P. Feynman, Phys. Rev. D 15, 2590 (1977).
[21]J. Whitmore, in *Proceedings of the 19th International Conference on High Energy Physics, Tokyo, 1978,* edited by S. Homma, M. Kawaguchi, and H. Miyazawa (Physical Society of Japan, Tokyo, 1979), p. 63.
[22]W. Ochs, Nucl. Phys. B118, 397 (1977).
[23]F. T. Dao *et al.*, Phys. Rev. Lett. 39, 1388 (1977).
[24]R. G. Roberts, R. C. Hwa, and S. Matsuda, J. Phys. G 5, 1043 (1979).
[25]A. Capella and A. Krzywicki, Phys. Rev D 18, 3357 (1978); Phys. Lett. 67B, 84 (1977).
[26]R. K. Shivpuri, Phys. Rev. D 15, 1926 (1977).
[27]C. Quigg, P. Pirila, and G. H. Thomas, Phys. Rev. Lett. 34, 290 (1975).
[28]Dale R. Snider, Phys. Rev. D 11, 140 (1975).
[29]C. Bromberg *et al.*, Phys. Rev. D 15, 1215 (1977); C. Bromberg *et al.*, *ibid.* 9, 1864 (1974); R. Singer *et al.*, Phys. Lett. 49B, 481 (1974); N. N. Biswas *et al.*, Phys. Rev. Lett. 35, 1059 (1975); T. Del Prete, Nuovo Cimento 5, 532 (1975); I. K. Daftari *et al.*, J. Phys. Soc. Jpn. 47, 349 (1979); L. Foa, Phys. Rep. 22C, 1 (1975).
[30]J. Whitmore, Phys. Rep. 27C, 187 (1976).
[31]V. P. Kenney, in *Proceedings of the 19th International Conference on High Energy Physics, Tokyo, 1978* (Ref. 21), p. 69.
[32]Chandra Gupt and R. K. Shivpuri, Lett. Nuovo Cimento 26, 88 (1979).